Nanoscale

PAPER

Cite this: *Nanoscale*, 2018, **10**, 7759

Ab initio quantum transport in polycrystalline graphene

Samuel Dechamps, * Viet-Hung Nguyen and Jean-Christophe Charlier*

Received 11th January 2018,
Accepted 21st March 2018

DOI: 10.1039/c8nr00289d

rsc.li/nanoscale

Synthesis techniques such as chemical vapor deposition yield graphene in polycrystalline flakes where single-crystal domains are separated by grain boundaries (GBs) of irregular shape. These structural defects are mostly made up of pentagon–heptagon pairs and represent an important source of scattering, thus strongly affecting electronic mobilities in polycrystalline graphene (PG). In the present article, first-principles simulations are performed to explore charge transport through a GB in PG using the Landauer–Büttiker formalism implemented within the Green's function approach. In ideal GB configurations, electronic transport is found to depend on their topology as already suggested in the literature. However, more realistic GBs constructed out of various carbon rings and with more complex periodicities are also considered, possibly inducing leakage currents. Finally, additional realistic disorder such as vacancies, a larger inter-connectivity region and out-of plane buckling is investigated. For specific energies, charge redistribution effects related to the detailed GB topology are found to substantially alter the transmissions. Altogether, the transport gap is predicted to be inversely proportional to the smallest significant periodic pattern and nearly independent of the interface configuration.

I. Introduction

In 2004, graphene was isolated by mechanical exfoliation from graphitic material,[2] triggering enormous enthusiasm in the scientific community due to its unusual properties. The peculiar physics in graphene arises from the confinement of electrons in two dimensions (2D). Interestingly, its low-energy charge carriers are massless chiral fermions with linear energy dispersion near the Brillouin zone corners, also called Dirac points.[3] Many exotic phenomena related to the singular nature of low-energy charge carriers were observed in graphene, such as room temperature half-integer quantum Hall effects[4] or Klein tunneling.[5] In addition, charge carriers are able to travel micrometer distances with negligible scattering.[6] The association of ballistic transport and low-energy linear dispersion with electron–hole symmetry, gapless character, and excellent gate controllability makes graphene an ideal platform for developing novel quantum devices based on unconventional concepts, such as valleytronics[7,8] or electronic optics.[7,9]

Although most of this novel 2D physics was firstly revealed on exfoliated monolayers, graphene is currently synthesized by chemical vapor deposition (CVD) techniques, which are presently by far the most viable and industry-compatible production methods.[10] Large-area wafer-scale monolayers can be transferred to desired substrates, patterned and modified locally, therefore enabling different electronic functionalities for all graphene-based circuits.[11] However, CVD graphene is found to be polycrystalline in nature hence composed of many single-crystal domains separated by grain boundaries (GBs) of irregular shapes. During CVD growth, grains nucleate on a substrate at different crystal-oriented sites and grow until line defects are formed at their intersection. Grain sizes range from a few hundred nanometers to several centimeters in diameter, with a roughness that mimics that of the substrate.[12] The line defects at the grain interface are mainly composed of topological defects that accommodate for the lattice mismatch between each domain. Particularly, GBs appear as extended structural defects consisting of a random one-dimensional distribution of non-hexagonal rings, mostly constituted of pentagon–heptagon pairs.[13] Scanning probe microscopy studies demonstrated that such one-dimensional defects introduce major perturbation in the electronic structure of graphene.[14,15] Indeed, these measurements revealed that GBs tend to be n-doped compared to the surrounding grains, thus acting as an electrical potential barrier for charge carriers.[16] Additionally, Kochat *et al.*[17] showed a strong correlation between the quality and the resistivity of GBs, with wide regions of disorder being more resistive than narrower ones. Tsen *et al.*[18] similarly established that poorly-connected GBs can significantly enhance the resistance of graphene by one order of magnitude, whereas Park *et al.*[19] concluded that the

Institute of Condensed Matter and Nanosciences, Université catholique de Louvain, Chemin des étoiles 8, B-1348 Louvain-la-Neuve, Belgium.
E-mail: samuel.dechamps@uclouvain.be, jean-christophe.charlier@uclouvain.be

electrical performance of well-stitched CVD graphene is not degraded by GBs. Lastly, transport measurement through GBs suggested that the resistance is temperature-independent, supporting the hypothesis that scattering at GBs is dominated by structural defects and impurities.[18,20] In summary, these structural defects strongly affect macroscopically the overall properties of wafer-scale graphene,[21] and GBs are known to be an important source of scattering that limit drastically the carrier mobility and consequently the performance of graphene-based electronic devices.[22] However, mobilities of 350 000 $cm^2\ V^{-1}\ s^{-1}$ were recently measured for CVD-grown graphene using advanced transfer techniques,[23] rivaling those obtained in both suspended[6] and encapsulated[24] graphene. These results suggest that CVD-grown graphene samples could be comparable in quality to large-area single-crystals obtained by exfoliation, which contain intragranular line defects and other structural imperfections.[25] Moreover, the controlled manufacturing of structurally well-defined line defects,[14] along with the potential to grow centimeter-sized single grains,[26] support the feasibility of designing novel CVD-grown graphene-based nano-devices.

In this context, the key role played by GBs on the transport properties of polycrystalline graphene (PG) is still a debated issue. So far, only a few theoretical studies based on the first-principles approach have tried to scrutinize the electronic transport through GBs but only for ideal or extremely specific geometries. Indeed, line of defects with rather short periodicities have been investigated,[1] demonstrating that their detrimental effect through atomically precise manufacturing could be removed, inducing the opening of a transport gap in PG which is of primary importance for switching off potential graphene-based nano-devices. However, these ideally aligned defects with short periodicities are not representative of real GBs which exhibit a more complicated atomic structure, neither straight nor periodic, and which are rather meandering aperiodic lines composed of fundamental units of pentagon–heptagon pairs with a significant amount of local disorder.[27] Consequently, the prediction of the transport properties in PG modeled with ideal GBs drastically deviates from experimental measurements.

In the present article, first-principles simulations based on density functional theory (DFT) are used to explore charge transport through a few "realistic" GBs. The GB atomic models are constructed using different types of geometries, with rather large periodicity and relatively complex non-hexagonal ring configurations in order to simulate as close as possible real GBs. The periodicity of GBs is analyzed through a perturbative approach while the inter-connectivity between grains is explored by considering diverse arrangements including vacancies, a larger inter-connectivity region and possible out-of-plane buckling, thus increasing local disorder step by step. For specific energies, charge redistribution effects related to the detailed GB topology are found to substantially alter the transmissions. Altogether, the transport gap is predicted to be inversely proportional to the smallest significant periodic pattern and nearly independent of the interface configuration, while disorder is found to induce leakage currents. The ambition is that this *ab initio* modeling of GBs will pave the way towards a more accurate understanding of their effect on the electronic transport in PG, which could in turn explain the almost-equivalent quality of CVD graphene compared to large-area single-crystals obtained by exfoliation.[23]

II. Methodology

First-principles calculations were conducted to compute electronic structures, as implemented in the OPENMX code.[28] The exchange–correlation energy and electron–ion interaction are described using the local-density approximation (LDA) and Troullier–Martins-type norm-conserving pseudopotentials,[29] respectively. First-principles calculations were performed with atomically localized basis functions decomposed in two s-orbitals and one p-orbital, denoted as "s2p1", while the energy cutoff for real-space mesh is set to 500 Ry. A fine k-point grid of $48 \times 48 \times 1$ for the graphene unit cell was employed using the Monkhorst–Pack scheme.[30] An interlayer vacuum distance of ~20 Å was used in order to avoid spurious image interaction.

Regarding the atomistic configurations, each graphene-based system was relaxed using classical molecular dynamics to minimize its configurational energy using optimized Tersoff potentials.[31] This empirical potential was demonstrated to accurately describe the structural, thermal and mechanical properties of PG.[32] The transport properties through GBs were computed using the Landauer–Büttiker formalism implemented within the Green's function (GF) approach. The scattering region enclosed by two semi-infinite leads spreads from 5 to 10 nm, in order to include most of the in-plane local strain caused by the atomic dislocation occurring in the GB vicinity. While this local strain affects to a slight extent the properties of electronic transport, its qualitative behavior as well as the transport gap are not significantly perturbed. Indeed, this gap is essentially due to the mismatch between the electronic structures of each domain, where the effects of the atomic dislocation are negligible.[33]

III. Results

In order to characterize structurally a GB as a periodic line of defects, some essential geometrical concepts should be specified (see Fig. 1). A translational vector $\mathbf{d}$ is used to relate the relative displacement between the lattices of the two graphene domains,[12,34] with a periodicity of 1–5 nm corresponding to periodically repeated atomic structures as experimentally observed in GBs.[1] In two-dimensional systems, $\mathbf{d}$ is expressed as (n_L,m_L) and (n_R,m_R) in the left and right graphene domains respectively. The (n_i,m_i) indexes describe the translational vector in terms of the lattice vectors $(\mathbf{a}_1,\mathbf{a}_2)$ in each crystalline region. In the left and right graphene domains, this vector is oriented by a respective angle θ_L and θ_R compared to a corresponding crystallographic direction (either armchair or zigzag). A total misorientation angle θ is defined with respect to the normal of the boundary line as $\theta = \theta_R + \theta_L$, based on the convention developed in ref. 35. In the following, two examples of

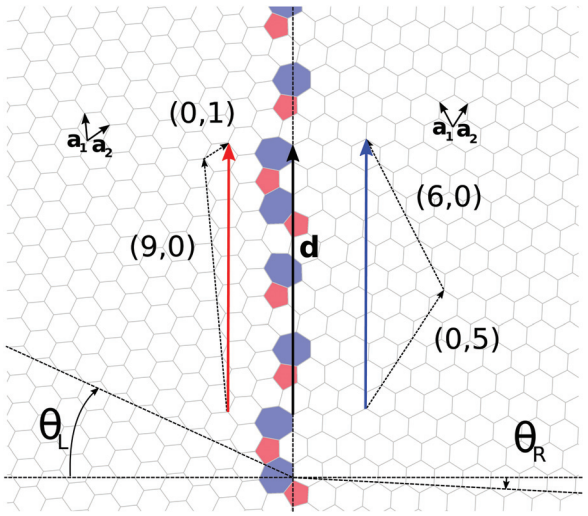

Fig. 1 Atomic structure of GBs in PG. An example of a GB containing four pentagon–heptagon pairs per unit cell and separating two graphene domains rotated compared to each other by $\theta = \theta_R + \theta_L = 21.8°$, where θ_L and θ_R represent the orientation of each domain with respect to the zigzag crystallographic direction. The same convention for misorientation angles was introduced in ref. 35. The translational vector **d** of the GB structure is defined by the matching vectors (9,1) and (6,5) in the left and right domains respectively, in terms of the lattice vectors (a_1,a_2) in each region.

GBs are reviewed in order to demonstrate the convenience of using the geometrical concepts illustrated in Fig. 1.

At first, the simplest case of a GB acting as a mirror symmetry line between two graphene domains is considered. Symmetric GBs exhibit a well-defined periodicity expressed as $|\mathbf{d}| = |(n_i, m_i)| = a_0\sqrt{(n_i^2 + n_i m_i + m_i^2)}$ where a_0 is the lattice parameter of graphene. This simple GB model is illustrated in Fig. 2a with a periodic alignment of pentagon–heptagon pairs. Pentagons lead to positive (spherical) curvature and heptagons to negative (saddle-like) curvature, such that a pentagon–heptagon pair lies inside the graphene plane. More generally, polygon curvatures must cancel each other as it results in a global warping with a logarithmically diverging energy.[36] Configurations of positive and negative structural defects are thus needed to cancel the curvature. Importantly, these structural defects conserve the three-fold coordination of each carbon atom and yield a low-energy cost for the GB.[12] In the present case, the dense sampling of pentagon–heptagon pairs corresponds to a large misorientation angle $\theta = 21.8°$ and a short periodicity $|\mathbf{d}| = 6.52$ Å (see Fig. 2a). Note that a small θ results in widely separated pentagon–heptagon pairs while a large θ induces the pairs to be close to each other. Simonis *et al.*[37] proposed this structural motif in the context of scanning tunneling microscopy studies of GBs in graphite. Its formation energy was estimated to be around 3.4 eV nm^{-1},[35]

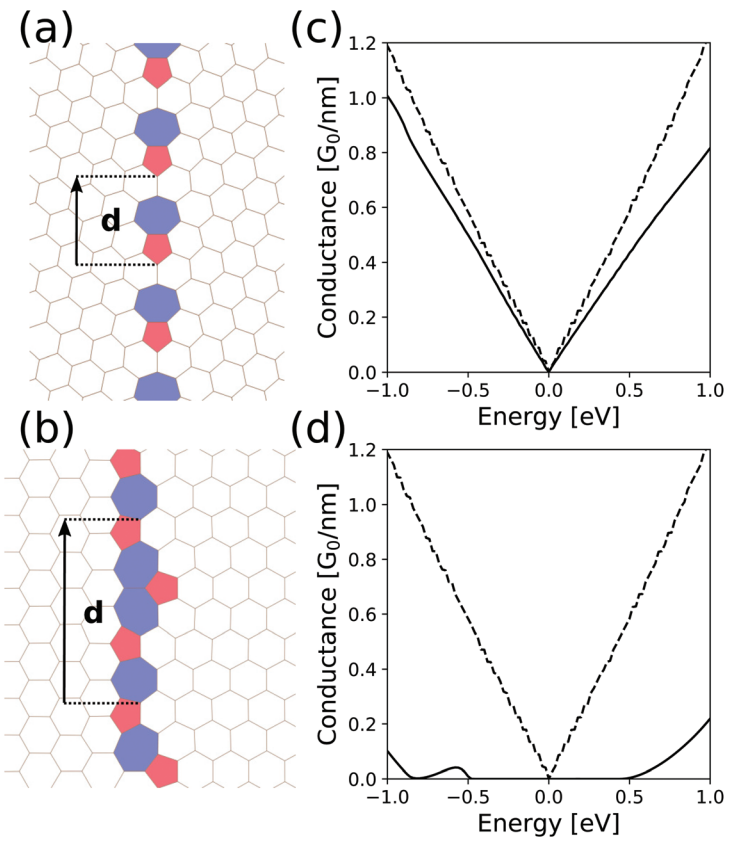

Fig. 2 First-principles electronic transport through ideal GBs in PG. Atomic structures of (a) the (2,1)|(2,1) ($\theta = 21.8°$) class-I GB and (b) the (5,0)|(3,3) ($\theta = 30.0°$) class-II GB with respective (c–d) zero-bias total conductance per unit length. Conductances through the GB as a function of energy (solid line) are compared to pristine graphene (dashed line).

which is much smaller than the typical formation energies of the bare graphene edges (about 10 eV nm^{-1} or more).[38]

A more general case involves an asymmetric GB with a periodicity that depends on specific commensurable conditions between the two graphene domains. The resulting period is typically much longer and usually induces a higher energy cost per unit length.[12,39] In order to reduce this energy cost, out-of-plane buckling might occur along the line defects to accommodate for the generated strain. The related buckling amplitude decreases with increasing misorientation angle and is typically around 1 Å along the out-of-plane direction.[35] Only planar topological defects are however considered hereafter, thus neglecting out-of-plane buckling. An example is depicted in Fig. 2b where the commensurable conditions are ensured by applying a relative strain between the two graphene grains. The misorientation angle is θ = 30.0° and the periodicity is set to $|\mathbf{d}|$ = 12.6 Å in order to distribute the stress equally between the left and right graphene domains, which are respectively oriented along the GB in the zigzag and armchair directions. Although the commensurable conditions involve a relative lattice mismatch $|\Delta\mathbf{d}|/|\mathbf{d}|$ = 3.85%, the corresponding atomic structure formation energy of 5.0 eV nm^{-1} is still considerably small,[35] indicating the relative stability of the asymmetric GB.

Yazyev and Louie[1] derived the transport properties across GBs using this structural description, where crossing an interface for charge carriers is equivalent to experiencing an effective rotation of the Brillouin zone. Importantly, GBs are assumed to be an infinitely long periodic array of defects. The electronic properties are derived solely for low-energy charge carriers, which are characterized by a linear energy dispersion around the Fermi energy. The dispersion relationship is thus written as $E(\mathbf{k}) = \hbar v_F|\mathbf{k}|$, where the Fermi velocity v_F and the momentum $\mathbf{k}$ are defined with respect to the Dirac points K and K' of the 2D Brillouin zone of graphene. Furthermore, crystal momentum conservation is assumed along the boundary line. Two cases are derived, depending on the expression of the translational vectors $\mathbf{d}$ in terms of the matching vectors (n_L,m_L) and (n_R,m_R). If $\mathbf{d}$ is expressed as $n - m = 3q$ with $q \in \mathbb{Z}$ for both domains (or equivalently as $n - m \neq 3q$), then for any charge carrier with a given momentum and energy in one domain, there exists a corresponding channel with the same momentum and energy in the other domain. However, if one translational vector belongs to $n - m = 3q$ whereas the other is defined as $n - m \neq 3q$, then the corresponding transmission is only feasible for certain allowed momentum and energy, thus inducing an effective transport gap for charge carriers. Subsequently, Yazyev and Louie[1] classified GBs in two categories, either transparent or reflective, labeled as class-I and class-II, respectively. The latter case is characterized by a transport gap defined such as:

$$E_g^* = \hbar v_F \frac{2\pi}{3|\mathbf{d}|} \approx \frac{1.38}{|\mathbf{d}|(nm)}\text{eV} \quad (1)$$

which depends exclusively on the boundary periodicity length ($|\mathbf{d}|$). This prediction suggests that GBs can be sorted based on their transport properties with information based only on their misorientation angle and periodicity. An important conclusion is that commensurable systems are class-I GBs whereas class-II GBs are incommensurable systems, thus characterized by a lattice mismatch.[1] The transport gap was later found to be sensitive to strain, with a dependence on the lattice symmetry of the two graphene domains surrounding the boundary.[33,40]

In this work, DFT calculations were performed with the basis set "s2p1", allowing for a less expensive computational cost but with the same accuracy level compared to ref. 1 where the basis set "s2p2d1" was used. Indeed, the conductances presented in Fig. 2 for the symmetric and asymmetric GBs are in very good agreement with those reported in Fig. 3 of ref. 1. Both configurations are characterized by small periodicities and large misorientation angles, indicating that the corresponding stable systems are planar. Line defects with $\theta \approx 30.0°$ are indeed predicted to remain flat for their ground-state configurations,[35] as also confirmed by our *ab initio* structural optimization with a force tolerance of 10^{-4} Ha a_0^{-1}. The symmetric class-I GB illustrated in Fig. 2a is defined by a linear combination of lattice vectors $\mathbf{d}$ = (2,1). The resulting total transmission for low-energy carriers exhibits a high transparency in Fig. 2c despite the large concentration of pentagon–heptagon pairs. The low scattering might be related to the atomically thin width of the interface. Note that there is a non-trivial asymmetry between holes and electrons, with a slightly larger conductance for holes. This small disparity is caused by the breaking of the bipartite symmetry of the graphene lattice for low-energy charge carriers due to the presence of topological defects, as already suggested in ref. 1. The computed transmission is in excellent agreement with the previously published results.[1,41,42] Regarding the asymmetric GB (see Fig. 2b), its translational vector is expressed in terms of lattice vectors $\mathbf{d}_L$ = (5,0) and $\mathbf{d}_R$ = (3,3). This system exhibits an extraordinarily large transport gap of E_g = 0.92 eV (see Fig. 2d), not so far from $E_g^* = 1.1$ eV estimated using eqn (1). Note that throughout the work, the value of the transport gap is determined in the logarithmic plot of conductances (see the details below) while it was estimated in the linear scale in ref. 1. This leads to a small difference between our reported value and the one obtained in ref. 1, although our method is the standard one to evaluate the capability of switching off the current in electronic devices. A parameter $\delta = \left(E_g^* - E_g\right)/E_g^*$ is consistently introduced, in order to measure the deviation between eqn (1) and DFT in further investigations. In this case, δ = 16.4%. Outside the transport gap, considerably smaller conductances for both electrons and holes are obtained compared to pristine graphene, with non-hexagonal rings breaking the electron–hole symmetry, in accordance once more with ref. 1. Overall, the transport properties across both commensurable and incommensurable GBs are found to be reasonably well characterized using the present numerical technique based on DFT, indicating that more complex configurations can be further investigated using this approach.

Consequently, a more realistic GB constructed from a more complicated arrangement of polygons is considered hereafter.

This array of point defects is characterized by the presence of dangling bonds, with a respective density of about 2 nm^{-1} (see Fig. 3a). Moreover, it is defined by a translational vector $|\mathbf{d}|$ = 32.0 Å, expressed as $\mathbf{d}_L$ = (11,3) and $\mathbf{d}_R$ = (10,5) in the graphene domains, which are tilted with respect to each other by θ = 30.8°. A relative lattice mismatch of $|\Delta\mathbf{d}|/|\mathbf{d}|$ = 3.55% is applied to ensure commensurability. Liu *et al.*[43] estimated the formation energy of a similar GB tilted by θ = 30.2° to be 4 eV nm^{-1}, thus indicating that the atomic structure illustrated in Fig. 3a should be relatively stable. When charge carriers cross the GB, this system is predicted to be transparent (see Fig. 3b), although the corresponding transmissions are relatively lower compared to pristine graphene. A damaging impact is supposedly due to the quality of the boundary, which contains dangling bonds that increase undesirable scattering of the charge carriers.

First-principles transport computations were then performed on class-II GBs. At first, an initial pattern defined by a periodicity $|\mathbf{d}|$ = 14.9 Å was considered, corresponding to $\mathbf{d}_L$ = (6,0) and $\mathbf{d}_R$ = (4,3) in the graphene domains (see Fig. 5a). This asymmetric GB is also characterized by a misorientation angle θ = 25.3°. From this simple configuration, more complicated GBs were constructed by removing an atom after repeating n times the initial pattern. The resulting relaxed configuration is thus interpreted as a periodic perturbation to the initial pattern. This perturbative analysis of disorder intends to benchmark the assumption to model GBs as a periodic line of defects. Indeed, most abundant GBs observed with the scanning tunneling microscope exhibit irregular structures, with no simple periodic array of dislocations.[15] In order to distinguish between different perturbed GBs, a nomenclature is introduced. The initial pattern illustrated in Fig. 5a is denoted as AMC-1d whereas any n-periodic system with an additional vacancy is denoted as AMC-nd. An example for n = 4 is depicted in Fig. 4a. Each disordered system corresponds to a vacancy concentration defined as $c = 0.673/n$ nm^{-1} for n = {1, 2, 3, 4}. The resulting conductances are presented in Fig. 4b. The semilogarithmic plot reveals non-zero currents as large as 10^{-2} G_0 nm^{-1} inside the transport gap as well as the presence of a secondary gap. A distinction is made by identifying the first as a *quasi* transport gap (QTG) and the second as a *real* transport gap (RTG), denoted as E_g. From eqn (1), it is evident that both gaps originate from two different periodicities. Indeed, the QTG is related to the initial pattern length $|\mathbf{d}|$ = 14.9 Å while the RTG is associated with the largest periodicity $|\mathbf{d}'| = n|\mathbf{d}|$ (see Fig. 4a). In contrast, non-zero transmissions are observed for AMC-3d with no dependence on the energy window, in agreement with the theoretical model. Inside the QTG, non-zero currents are identified as leakage currents, whose occurrence was predicted in the presence of randomly distributed impurities.[1] The leakage currents observed in ref. 1 were computed using a tight-binding (TB) model for a supercell with a periodicity of 11 nm and impurity concentrations ranging from 0.1 to 1 nm^{-1}. Such concentrations are equivalent to the vacancy densities of AMC-nd which run from 0.2 to 0.7 nm^{-1}. Outside the QTG, conductances appear to be similar and independent of the vacancy concentration, with a transparency of about 30% compared to pristine graphene. Afterwards, the RTG is estimated for n = {1, 2, 4} using a tolerance criterion of 10^{-5} G_0 nm^{-1}, which corresponds to leakage current as small as 10^{-2} G_0 nm^{-1} with an I_{on}/I_{off} ratio of 10^3 as typically used in the literature.[44] The transmission gaps extracted from *ab initio* calculations are summarized in Table 1 and compared to values computed from eqn (1). A qualitative agreement is observed between E_g and the theoretical predictions, with a nearly constant deviation parameter not so far from the previously estimated $\delta \approx 16\%$. Importantly, the proportional trend between E_g and $1/n$ is well represented.

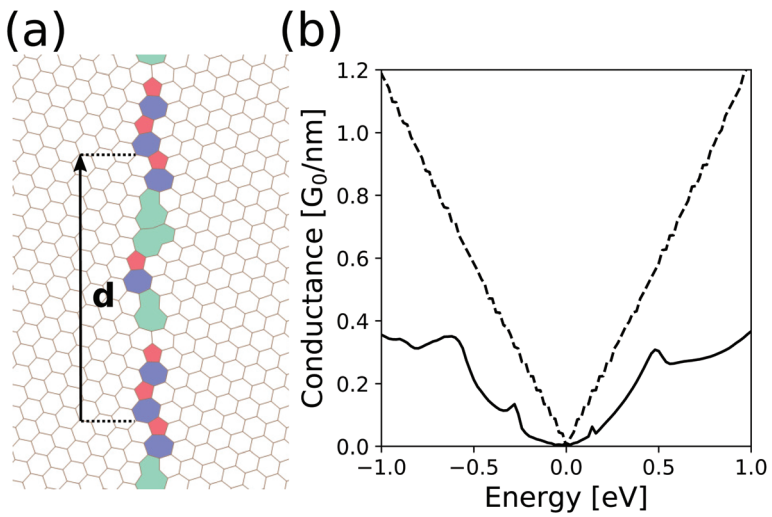

Fig. 3 First-principles electronic transport through a realistic GB in PG. (a) Atomic structure of the (11,3)|(10,5) (θ = 30.8°) class-I GB where the pentagon (red) and heptagon (blue) are highlighted in green when the pair contains a dangling bond. (b) Zero-bias total conductance per unit length through the GB as a function of energy (solid line) compared to pristine graphene (dashed line).

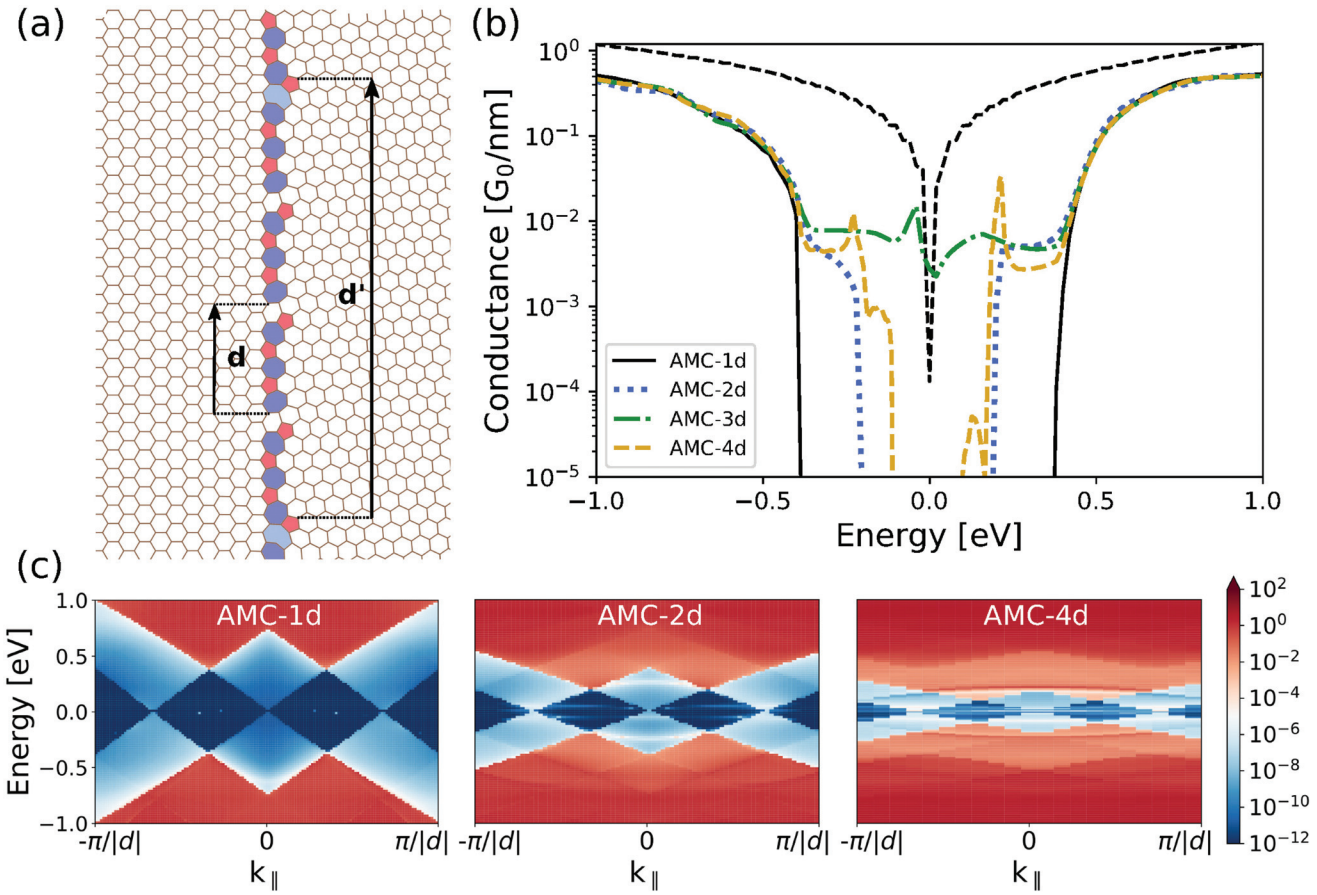

Fig. 4 First-principles electronic transport through even more realistic GBs in PG. (a) Atomic structure of the (24,0)|(16,12) (θ = 25.3°) class-II GB (denoted as AMC-4d) where a carbon ring containing a vacancy is highlighted in azure. The initial and the repeated periodicities are respectively defined as |**d**| = 14.9 Å and |**d**′| = 4|**d**|. (b) Zero-bias total conductance per unit length through AMC-*n*d with *n* = {1, 2, 3, 4} as a function of energy compared to pristine graphene (black dashed line). (c) Transmission probabilities (in logarithmic units) as a function of transverse momentum $k_{\parallel}$ and energy *E* for AMC-1d, AMC-2d and AMC-4d (from left to right).

Table 1 Transmission gaps extracted from *ab initio* calculations (E_g) and computed from eqn (1) $\left(E_g^*\right)$, with the corresponding relative deviation $\delta = \left(E_g^* - E_g\right)/E_g^*$

	E_g [eV]	E_g^* [eV]	δ [%]
AMC-1d	0.76	0.93	18
AMC-2d	0.38	0.46	17
AMC-4d	0.20	0.23	13

Note that for certain transport-forbidden momentum and energy, maxima in transmissions are observed in the form of flat energy lines which are well perceptible in the case of AMC-2d for $k_{\parallel}/|\mathbf{d}| \in [-\pi/3, +\pi/3]$ and $E \approx 0.3$ eV (see Fig. 4c). Those peaks however result from numerical errors in the GF calculations, due to the presence of electronic states strongly localized in space and unequivocally related to the one-dimensional nature of line defects.[15,45,46]

Afterwards, the primary mechanisms of scattering of charge carriers at GBs are identified, in accordance with experimental observations. STM and STS measurements revealed that GBs perturb greatly the local electronic structure due to charge redistribution effects that depend explicitly on structural considerations.[15] The scattering of charge carriers is therefore expected to be influenced non-trivially by many atomistic parameters.[47] Some predominant features can however be determined. At first, intrinsic topological defects are found to generate localized states at the Dirac point,[14,35,45] which result in resonant backscattering of low-energy charge carriers.[48] STM measurements also indicate that the resistance of GBs is changing with the width of the scattering region.[17,18,49] Finally, introducing corrugation is expected to bear important implications on the transport properties in PG.[50] Consequently, the electronic transport of AMC-1d can be perturbed with additional disorder in the form of: (1) highly concentrated vacancies, (2) a larger inter-connectivity region (LIR) and (3) out-of-plane buckling. The resulting atomic configurations are illustrated in Fig. 5a–f and the corresponding conductances are depicted in Fig. 5g. The effects of vacancies are investigated with two boundaries characterized by a concentration of vacancy $c_i^* = i0.67$ nm^{-1} where $i = \{1, 2\}$. Note that introducing a vacancy in a hexagonal network creates three dangling

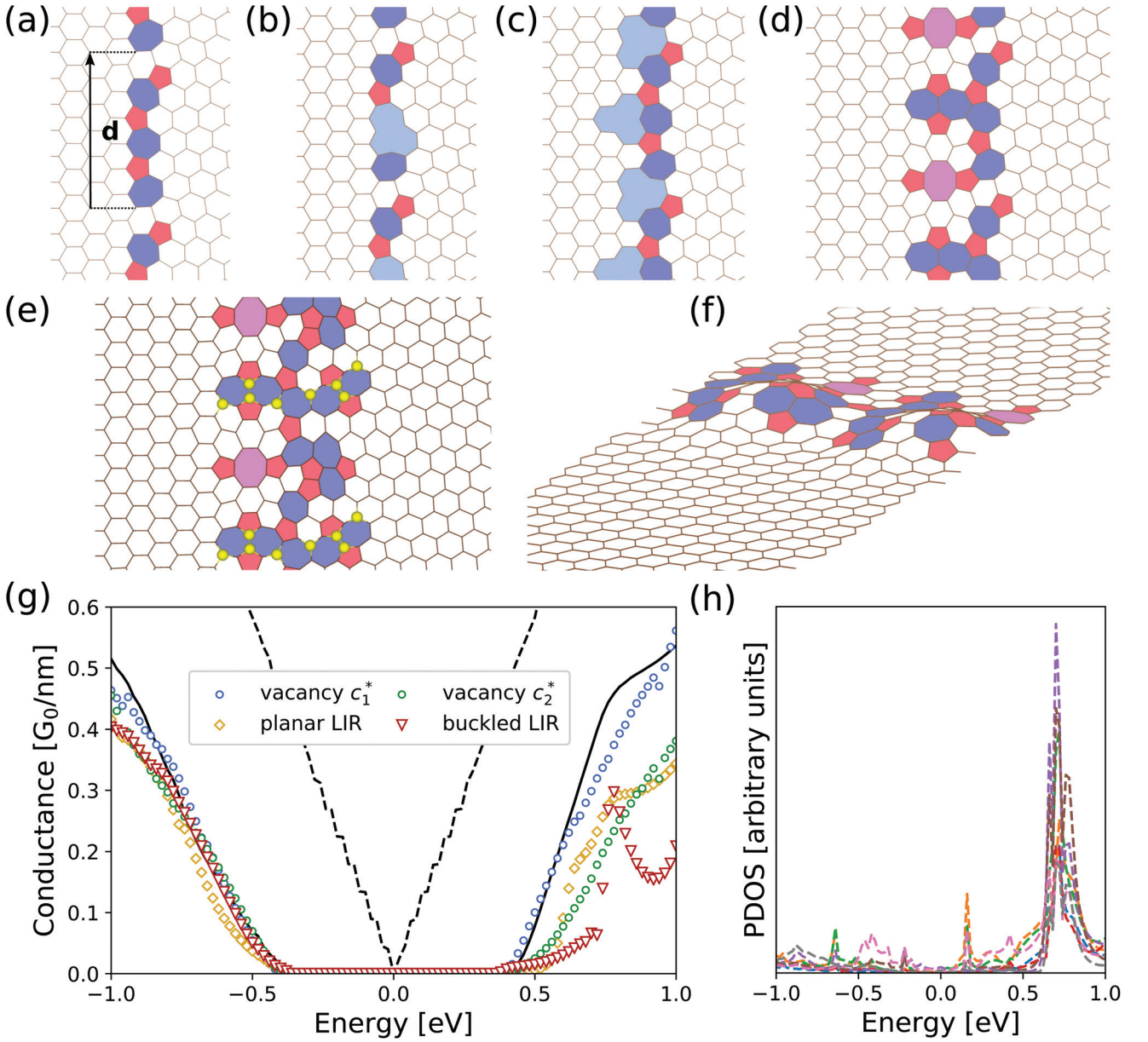

Fig. 5 First-principles electronic transport through disordered and buckled GBs in PG. Atomic structures of the (6,0)|(4,3) (θ = 25.3°) class-II GB for (a) the initial pattern, (b–c) with highly concentrated vacancies (c_1^* and c_2^*), (d–f) with larger inter-connectivity regions (LIR) (d) for planar geometry and (e–f) out-of-plane buckling (respective top and side views). A carbon ring containing a vacancy is highlighted in azure while pentagons, heptagons and octagons are displayed in red, blue and purple, respectively. (g) Zero-bias total conductance per unit length through these disordered GBs as a function of energy compared to the ones of pristine graphene (black dashed line) and of the initial pattern (black solid line) (h) Projected density of states (PDOS) as a function of energy corresponding to carbon atoms highlighted in yellow in (e).

bonds, which will eventually relax to form energetically more stable reconstructed vacancies, as demonstrated by structural geometric optimization using first-principles.[51] However, the three-dangling-bond configuration has been preserved here to enhance the vacancy detrimental effects in the scope of charge transport. Regarding the computed transmissions, no notable impact is noticed concerning c_1^*, although the induced modification to scattering results in small enhancements or diminutions in conductance at specific energies. Note that no perceptible effect was observed for AMC-*n*d with slightly lower vacancy concentrations. In contrast, a uniform drop in the electronic conductances of at most 50% occurs for c_2^* due to the large concentration of vacancies. When considering larger inter-connectivity regions, electronic transmissions are also reduced on average by 50% and 75% for the planar and the buckled systems respectively. These predictions seem to be in good agreement with experimental measurements for poorly-connected grains.[18] Additionally, a transmission peak is found to appear at $E \approx 0.8$ eV in the case of out-of-plane buckling, suggesting that local electronic perturbations might improve

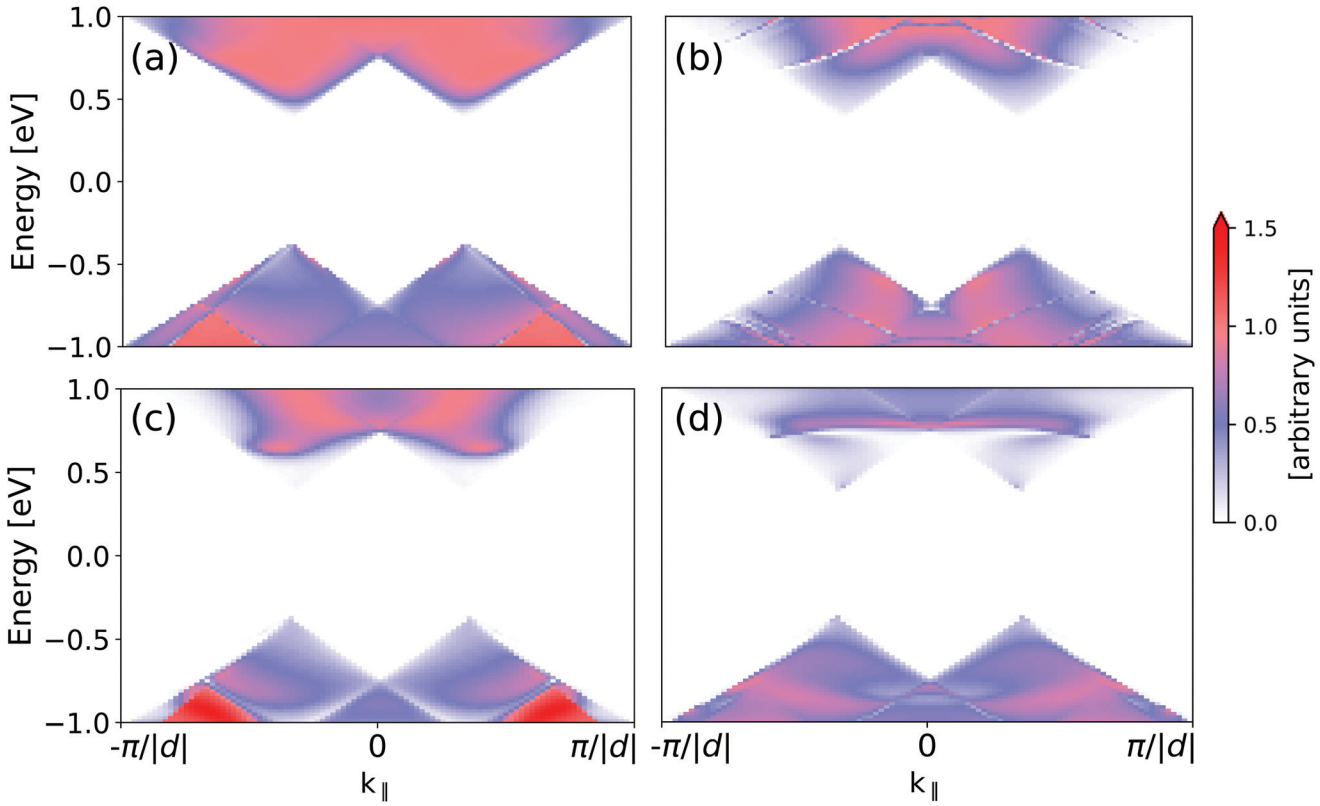

Fig. 6 Transmission probabilities of the (6,0)|(4,3) (θ = 25.3°) class-II GB as a function of transverse momentum $k_{\|}$ and energy E for (a) the initial pattern, (b) highly concentrated vacancies (c_2^*), a larger inter-connectivity region with (c) planar geometry and (d) out-of-plane buckling (for the corresponding atomic structures see Fig. 5).

electronic transport for specific energies as suggested in ref. 46 and 52. To clarify the role of these charge redistribution effects, the local density of states (DOS) is investigated inside the scattering region. For the case of buckled AMC-1d, a maximum in the DOS is found at $E \approx 0.8$ eV (see Fig. 5h), in agreement with the experimental observation that periodic GBs give sharp DOS peaks.[53] This peak can be unambiguously associated with a series of atoms distributed along a line of heptagons (see the highlight in Fig. 5e), indicating that such odd-membered rings induce resonant states slightly above the Fermi energy as previously suggested in carbon nanotubes.[54] Since an enhancement in the DOS non-orthogonal to transport is unequivocally related in the GF formalism to an increase in transmissions, the charge redistribution effects due to this chain of heptagons are found to enhance the total conductance at $E \approx 0.8$ eV. Concerning the transmissions of holes, conductances are observed to be weakly sensitive to the type of disorder (Fig. 5g). However, an investigation of the transmission probabilities (see Fig. 6) indicates that scattering modifies differently the transport behavior in each defective system, with a non-trivial dependence on the energy and the momentum $k_{\|}$ of the charge carrier. Therefore, the transmission of holes is found to be significantly sensitive to the nature of defects whereas the obtained conductances are only slightly affected in the considered cases due to the contribution of all momenta $k_{\|}$. Lastly, the transport gap is found to remain constant despite the type of disorder for a tolerance criterion of 10^{-3} G_0 nm^{-1}, in agreement with eqn (1). Note however that transmissions are decreased by one order of magnitude at $E \approx 0.5$ eV for larger inter-connectivity regions, indicating that an effective transport gap would depend not only on $|\mathbf{d}|$ but also on the detailed GB topology.[41]

IV. Conclusion

In summary, both metallic and semi-conducting transport behaviors were obtained *ab initio* for two simple cases, as previously reported in the literature.[1] For more realistic semi-conducting GBs, the transport gap was shown to be qualitatively consistent with theoretical predictions, with a well-defined inverse dependence on the periodicity.

The effects of disorder on charge transport were investigated afterwards by considering more complex configurations, including non-hexagonal rings, vacancies, larger inter-connectivity regions with planar and buckled geometries, in order to simulate GBs as close as possible to experimental observations. The transmission of transparent GBs was reported to be sensitively reduced in the presence of non-hexagonal rings of carbon atoms, thus increasing the

scattering of charge carriers due to a lesser inter-connectivity between grains. When adding periodically repeated vacancies to an enlarged initial pattern, leakage currents as large as 10^{-2} G_0 nm^{-1} were observed in the case of reflective GBs. However, the transport gap associated with the smallest apparent periodicity was found to be nearly independent of the presence of vacancies, a larger inter-connectivity region or out-of-plane buckling. Outside this transmission gap, the effect of disorder was reported to be negligible for holes and an overall decrease as large as 75% was noticed for electrons in the case of a large concentration of defects with out-of-plane buckling. For specific energies, transmissions were found to be substantially decreased or increased, depending on the charge redistribution effects related to the detailed GB topology.

Random disorder is found to normalize the transport behavior in PG. On one hand, imperfections tend in general to enhance scattering effects which in turn reduce the overall transmission of transparent systems. On the other hand, the reflective character fades away in disordered reflective systems due to the emergence of leakage currents. Moreover, non-zero transmissions for both classes of GBs are difficult to quantify, due to the non-trivial scattering that depends on the unique characteristics of the boundary. In consequence, experimental conductances are presumably quite universal and robust,[27] independently of the theoretically predicted metallic or semiconducting transport regimes. Furthermore, the finding of robust conductances decreasing moderately even for large concentrations of defects supports the observation of an almost-equivalent quality of CVD graphene compared to large-area single-crystals obtained by exfoliation.[23]

Finally, it is important to note that disorder was always periodically repeated in the present study. However, structural irregularities are intrinsically non-periodic as GBs resemble more or less dissimilarly to periodic arrays of point defects. This discrepancy could possibly induce a small perturbation of the formerly stated results based on a periodicity assumption. Additionally, the considered imperfections (see Fig. 5b–f) represent a non-exhaustive variety of disorder, which might not describe all the possible effects of disorder. For example, chemical functionalization could have been investigated in order to describe more completely scattering mechanisms occurring at GBs. Indeed, Seifert *et al.*[55] suggested that the electronic properties of PG are largely dependent on the nature of functional groups, which are intrinsically present at GBs due to their high chemical reactivity. Despite these limitations, the present results represent an improvement at the atomistic scale in the understanding of the transport properties through the GBs in PG, whose characterization might pave the way towards important practical applications for all-graphene-based electronics.

Conflicts of interest

There are no conflicts to declare.

Acknowledgements

The authors would like to thank Dr A. Lherbier and B. Van Troeye for fruitful scientific discussions. The authors acknowledge financial support from the Fédération Wallonie-Bruxelles through the ARC entitled 3D Nanoarchitecturing of 2D crystals (No. 16/21-077), from the European Union's Horizon 2020 research and innovation programme (No. 696656), and from the Belgium F.R.S-FNRS under the conventions No. T.0051.18 and T.1077.15. Computational resources have been partly provided by the supercomputing facilities of the Université catholique de Louvain (CISM/UCL) and the Consortium des Equipements de Calcul Intensif en Fédération Wallonie Bruxelles (CECI) funded by the Fonds de la Recherche Scientifique de Belgique (F.R.S-FNRS) under the convention No. 2.5020.11.

References

1 O. V. Yazyev and S. G. Louie, *Nat. Mater.*, 2010, **9**, 806–809.
2 K. S. Novoselov, A. K. Geim, S. V. Morozov, D. Jiang, Y. Zhang, S. V. Dubonos, I. V. Grigorieva and A. A. Firsov, *Science*, 2004, **306**, 666–669.
3 A. C. Neto, F. Guinea, N. M. Peres, K. S. Novoselov and A. K. Geim, *Rev. Mod. Phys.*, 2009, **81**, 109.
4 K. S. Novoselov, A. K. Geim, S. V. Morozov, D. Jiang, M. I. Katsnelson, I. V. Grigorieva, S. V. Dubonos and A. A. Firsov, *Nature*, 2005, **438**, 197–200.
5 M. Katsnelson, K. Novoselov and A. Geim, *Nat. Phys.*, 2006, **2**, 620–625.
6 K. I. Bolotin, K. Sikes, Z. Jiang, M. Klima, G. Fudenberg, J. Hone, P. Kim and H. Stormer, *Solid State Commun.*, 2008, **146**, 351–355.
7 V. H. Nguyen, S. Dechamps, P. Dollfus and J.-C. Charlier, *Phys. Rev. Lett.*, 2016, **117**, 247702.
8 A. Rycerz, J. Tworzydlo and C. Beenakker, *Nat. Phys.*, 2007, **3**, 172; D. Xiao, W. Yao and Q. Niu, *Phys. Rev. Lett.*, 2007, **99**, 236809; D. Gunlycke and C. T. White, *Phys. Rev. Lett.*, 2011, **106**, 136806.
9 V. V. Cheianov, V. Fal'ko and B. Altshuler, *Science*, 2007, **315**, 1252; J. Williams, T. Low, M. Lundstrom and C. Marcus, *Nat. Nanotechnol.*, 2011, **6**, 222; P. e. a. Rickhaus, *Nat. Commun.*, 2013, **4**, 2342.
10 M. S. A. Bhuyan, M. N. Uddin, M. M. Islam, F. A. Bipasha and S. S. Hossain, *Int. Nano Lett.*, 2016, **6**, 65–83.
11 K. S. Novoselov, V. Fal, L. Colombo, P. Gellert, M. Schwab, K. Kim, *et al.*, *Nature*, 2012, **490**, 192–200.
12 A. Isacsson, A. W. Cummings, L. Colombo, L. Colombo, J. M. Kinaret and S. Roche, *2D Mater.*, 2016, **4**, 012002.
13 P. Y. Huang, C. S. Ruiz-Vargas, A. M. van der Zande, W. S. Whitney, M. P. Levendorf, J. W. Kevek, S. Garg, J. S. Alden, C. J. Hustedt, Y. Zhu, *et al.*, *Nature*, 2011, **469**, 389; K. Kim, Z. Lee, W. Regan, C. Kisielowski, M. Crommie and A. Zettl, *ACS Nano*, 2011, **5**, 2142.

14 J. Lahiri, Y. Lin, P. Bozkurt, I. I. Oleynik and M. Batzill, *Nat. Nanotechnol.*, 2010, **5**, 326–329.

15 A. Luican-Mayer, J. E. Barrios-Vargas, J. T. Falkenberg, G. Autès, A. W. Cummings, D. Soriano, G. Li, M. Brandbyge, O. V. Yazyev, S. Roche, *et al.*, *2D Mater.*, 2016, **3**, 031005.

16 J. C. Koepke, J. D. Wood, D. Estrada, Z.-Y. Ong, K. T. He, E. Pop and J. W. Lyding, *ACS Nano*, 2013, **7**, 75; H. Song, S. Li, H. Miyazaki, S. Sato, K. Hayashi, A. Yamada, N. Yokoyama and K. Tsukagoshi, *Sci. Rep.*, 2012, **2**, 337.

17 V. Kochat, C. S. Tiwary, T. Biswas, G. Ramalingam, K. Hsieh, K. Chattopadhyay, S. Raghavan, M. Jain and A. Ghosh, *Nano Lett.*, 2015, **16**, 562–567.

18 A. W. Tsen, L. Brown, M. P. Levendorf, F. Ghahari, P. Y. Huang, R. W. Havener, C. S. Ruiz-Vargas, D. A. Muller, P. Kim and J. Park, *Science*, 2012, **336**, 1143–1146.

19 S. Park, M. A. Shehzad, M. F. Khan, G. Nazir, J. Eom, H. Noh and Y. Seo, *Carbon*, 2017, **112**, 142–148.

20 Y. Ogawa, K. Komatsu, K. Kawahara, M. Tsuji, K. Tsukagoshi and H. Ago, *Nanoscale*, 2014, **6**, 7288–7294.

21 A. W. Cummings, D. L. Duong, V. L. Nguyen, D. Van Tuan, J. Kotakoski, J. E. Barrios Vargas, Y. H. Lee and S. Roche, *Adv. Mater.*, 2014, **26**, 5079–5094.

22 D. Van Tuan, J. Kotakoski, T. Louvet, F. Ortmann, J. C. Meyer and S. Roche, *Nano Lett.*, 2013, **13**, 1730; Q. Yu, L. A. Jauregui, W. Wu, R. Colby, J. Tian, Z. Su, H. Cao, Z. Liu, D. Pandey, D. Wei, *et al.*, *Nat. Mater.*, 2011, **10**, 443; A. Kumari, N. Prasad, P. Bhatnagar, P. Mathur, A. K. Yadav, C. Tomy and C. Bhatia, *Diamond Relat. Mater.*, 2014, **45**, 28.

23 L. Banszerus, M. Schmitz, S. Engels, J. Dauber, M. Oellers, F. Haupt, K. Watanabe, T. Taniguchi, B. Beschoten and C. Stampfer, *Sci. Adv.*, 2015, **1**, e1500222.

24 A. S. Mayorov, R. V. Gorbachev, S. V. Morozov, L. Britnell, R. Jalil, L. A. Ponomarenko, P. Blake, K. S. Novoselov, K. Watanabe, T. Taniguchi, *et al.*, *Nano Lett.*, 2011, **11**, 2396–2399.

25 H. Zhou, W. J. Yu, L. Liu, R. Cheng, Y. Chen, X. Huang, Y. Liu, Y. Wang, Y. Huang and X. Duan, *Nat. Commun.*, 2013, **4**, 2096.

26 T. Wu, X. Zhang, Q. Yuan, J. Xue, G. Lu, Z. Liu, H. Wang, H. Wang, F. Ding, Q. Yu, *et al.*, *Nat. Mater.*, 2016, **15**, 43–47.

27 L. Tapasztó, P. Nemes-Incze, G. Dobrik, K. Jae Yoo, C. Hwang and L. P. Biró, *Appl. Phys. Lett.*, 2012, **100**, 053114.

28 T. Ozaki, *Phys. Rev. B: Condens. Matter*, 2003, **67**, 155108; T. Ozaki and H. Kino, *Phys. Rev. B: Condens. Matter*, 2004, **69**, 195113; T. Ozaki and H. Kino, *Phys. Rev. B: Condens. Matter*, 2005, **72**, 045121.

29 N. Troullier and J. L. Martins, *Phys. Rev.*, 1993, **43**, 1991.

30 H. J. Monkhorst and J. D. Pack, *Phys. Rev. B: Solid State*, 1976, **13**, 5188.

31 J.-W. Jiang, B.-S. Wang, J.-S. Wang and H. S. Park, *J. Phys.: Condens. Matter*, 2015, **27**, 083001.

32 L. Lindsay and D. Broido, *Phys. Rev. B: Condens. Matter*, 2010, **81**, 205441.

33 V. H. Nguyen, T. X. Hoang, P. Dollfus and J.-C. Charlier, *Nanoscale*, 2016, **8**, 11658–11673.

34 G. Gottstein, *Physical foundations of materials science*, Springer Science & Business Media, 2013.

35 O. V. Yazyev and S. G. Louie, *Phys. Rev. B: Condens. Matter*, 2010, **81**, 195420.

36 H. Seung and D. R. Nelson, *Phys. Rev. A*, 1988, **38**, 1005.

37 P. Simonis, C. Goffaux, P. Thiry, L. Biro, P. Lambin and V. Meunier, *Surf. Sci.*, 2002, **511**, 319–322.

38 P. Koskinen, S. Malola and H. Häkkinen, *Phys. Rev. Lett.*, 2008, **101**, 115502.

39 J. Zhang and J. Zhao, *Carbon*, 2013, **55**, 151–159.

40 S. B. Kumar and J. Guo, *Nano Lett.*, 2012, **12**, 1362–1366.

41 J. Zhang, J. Gao, L. Liu and J. Zhao, *J. Appl. Phys.*, 2012, **112**, 053713.

42 H. Zhang, G. Lee, C. Gong, L. Colombo and K. Cho, *J. Phys. Chem. C*, 2014, **118**, 2338–2343.

43 T.-H. Liu, G. Gajewski, C.-W. Pao and C.-C. Chang, *Carbon*, 2011, **49**, 2306–2317.

44 G. Fiori, F. Bonaccorso, G. Iannaccone, T. Palacios, D. Neumaier, A. Seabaugh, S. K. Banerjee and L. Colombo, *Nat. Nanotechnol.*, 2014, **9**, 768–779.

45 A. Mesaros, S. Papanikolaou, C. Flipse, D. Sadri and J. Zaanen, *Phys. Rev. B: Condens. Matter*, 2010, **82**, 205119.

46 C. Ma, H. Sun, Y. Zhao, B. Li, Q. Li, A. Zhao, X. Wang, Y. Luo, J. Yang, B. Wang, *et al.*, *Phys. Rev. Lett.*, 2014, **112**, 226802.

47 S. Ihnatsenka and I. Zozoulenko, *Phys. Rev. B: Condens. Matter*, 2013, **88**, 085436.

48 F. Gargiulo and O. V. Yazyev, *Nano Lett.*, 2013, **14**, 250–254.

49 K. W. Clark, X.-G. Zhang, I. V. Vlassiouk, G. He, R. M. Feenstra and A.-P. Li, *ACS Nano*, 2013, **7**, 7956–7966.

50 A. Capasso, E. Placidi, H. Zhan, E. Perfetto, J. M. Bell, Y. Gu and N. Motta, *Carbon*, 2014, **68**, 330–336.

51 G.-D. Lee, C. Wang, E. Yoon, N.-M. Hwang, D.-Y. Kim and K. Ho, *Phys. Rev. Lett.*, 2005, **95**, 205501.

52 J. Sun, N. Lin, Z. Li, H. Ren, C. Tang and X. Zhao, *RSC Adv.*, 2016, **6**, 1090–1097.

53 B. Yang, H. Xu, J. Lu and K. P. Loh, *J. Am. Chem. Soc.*, 2014, **136**, 12041–12046.

54 J.-C. Charlier, T. Ebbesen and P. Lambin, *Phys. Rev. B: Condens. Matter*, 1996, **53**, 11108.

55 M. Seifert, J. E. Vargas, M. Bobinger, M. Sachsenhauser, A. W. Cummings, S. Roche and J. A. Garrido, *2D Mater.*, 2015, **2**, 024008.